Mineralogical Magazine (2020), **84**, 81–91
doi:10.1180/mgm.2019.64

CAMBRIDGE UNIVERSITY PRESS

Article

Mineralogy and genesis of pyrochlore apatitite from The Good Hope Carbonatite, Ontario: A potential niobium deposit

Roger H. Mitchell[1]*, Rudy Wahl[2] and Anthony Cohen[3]

[1]Department of Geology, Lakehead University, Thunder Bay, Ontario, Canada P7B 5E1; [2]The Wahl Prospecting Group, Box 1022, Marathon, Ontario, P0T 2E0; and [3]Plato Gold Corp 1240 Bay Street, Suite 800, Toronto, Ontario, M5R 2A7

Abstract

The Good Hope carbonatite is located adjacent to the Prairie Lake alkaline rock and carbonatite complex in northwestern Ontario. The occurrence is a heterolithic breccia consisting of diverse calcite, dolomite and ferrodolomite carbonatites containing clasts of magnesio-arfvedsonite + potassium feldspar, phlogopite + potassium feldspar together with pyrochlore-bearing apatitite clasts. The apatitite occurs as angular, boudinaged and schlieren clasts up to 5 cm in maximum dimensions. In these pyrochlore occurs principally as euhedral single crystals (0.1–1.5 cm) and can comprise up to 25 vol.% of the clasts. Individual clasts contain compositionally- and texturally-distinct suites of pyrochlore. The pyrochlores are hosted by small prismatic crystals of apatite (~100–500 μm × 10–25 μm) that are commonly flow-aligned and in some instances occur as folds. Allotriogranular cumulate textures are not evident in the apatitites. The fluorapatite does not exhibit compositional zonation under back-scattered electron spectroscopy, although ultraviolet and cathodoluminescence imagery shows distinct cores with thin (<50 μm) overgrowths. Apatite lacks fluid or solid inclusions of other minerals. The apatite is rich in Sr (7030–13,000 ppm) and rare earth elements and exhibits depletions in La, Ce, Pr and Nd (La/Nd_{CN} ratios (0.73–1.14) relative to apatite in cumulate apatitites (La/Nd_{CN} > 1.5) in the adjacent Prairie Lake complex. The pyrochlore are primarily Na–Ca pyrochlore of relatively uniform composition and minor Sr contents (<2 wt.% SrO). Irregular resorbed cores of some pyrochlores are *A*-site deficient (>50%) and enriched in Sr (6–10 wt.% SrO), BaO (0.5–3.5 wt.%), Ta_2O_5 (1–2 wt.%) and UO_2 (0.5–2 wt.%). Many of the pyrochlores exhibit oscillatory zoning. Experimental data on the phase relationships of haplocarbonatite melts predicts the formation of apatite and pyrochlore as the initial liquidus phases in such systems. However, the texture of the clasts indicates that pyrochlore and apatite did not crystallise together and it is concluded that pyrochlores formed in one magma have been mechanically mixed with a different apatite-rich magma. Segregation of the apatite–pyrochlore assemblage followed by lithification resulted in the apatitites, which were disrupted and fragmented by subsequent batches of diverse carbonatites. The genesis of the pyrochlore apatitites is considered to be a process of magma mixing and not simple *in situ* crystallisation.

Keywords: pyrochlore, apatite, apatitite, carbonatite, magma mixing

(Received 13 August 2019; accepted 27 September 2019; Accepted Manuscript published online: 04 October 2019; Associate Editor: Sam Broom-Fendley)

Introduction

Niobium (Nb) has a wide variety of uses ranging from niobium carbide- and nitride-steel alloys though diverse piezoelectric compounds to superconducting Nb–Sn magnets. Niobium is regarded as a 'critical or strategic metal' in that although it has numerous industrial uses there are few exploitable sources. Currently, there are only three major operating Nb mines (Araxa and Catalão-II in Brazil and St. Honoré, Canada). The Brazilian deposits account for ~92% of total worldwide production with St. Honoré and other sources (e.g. Lovozero, Russia; Pitinga, Brazil) for 7 and 1%, respectively. Accordingly, there is great interest in developing new sources of Nb and to that end many occurrences in carbonatites are being evaluated [e.g. Aley, Upper Fir and Eldor (Canada); Elk Creek (Nebraska, USA); Tomtor (Russia)] or re-evaluated [e.g. Oka, James Bay (Canada); Fen (Norway); Panda Hill, Ngualla (Tanzania)]. Brazil has significant Nb reserves at Seis Lagos, Tapira and Salitre, together with the decommissioned mine at Catalão-I (Mitchell, 2015).

One objective of this contribution is to draw attention to a significant potential source of Nb in the Good Hope Carbonatite located in northwestern Ontario (Canada) and to the unusual character of the mineralisation. In common with other Nb deposits pyrochlore is the main ore mineral, however at Good Hope it occurs principally as pyrochlore-apatitite clasts rather than as a disseminated phase in carbonatite. Description of these clasts and presentation of a hypothesis for their genesis is the principal objective of this contribution.

Geological setting

The Good Hope carbonatite is a satellite intrusion of the well-known Prairie Lake alkaline rock and carbonatite complex (Sage, 1987; Zurevinski and Mitchell, 2015; Wu *et al.*, 2017),

*Author for correspondence: Roger H. Mitchell. Email: rmitchel@lakeheadu.ca
This paper is part of a thematic set arising from the 3rd International Critical Metals Conference (Edinburgh, May 2019).
Cite this article: Mitchell R.H., Wahl R. and Cohen A. (2020) Mineralogy and genesis of pyrochlore apatitite from The Good Hope Carbonatite, Ontario: A potential niobium deposit. *Mineralogical Magazine* **84**, 81–91. https://doi.org/10.1180/mgm.2019.64

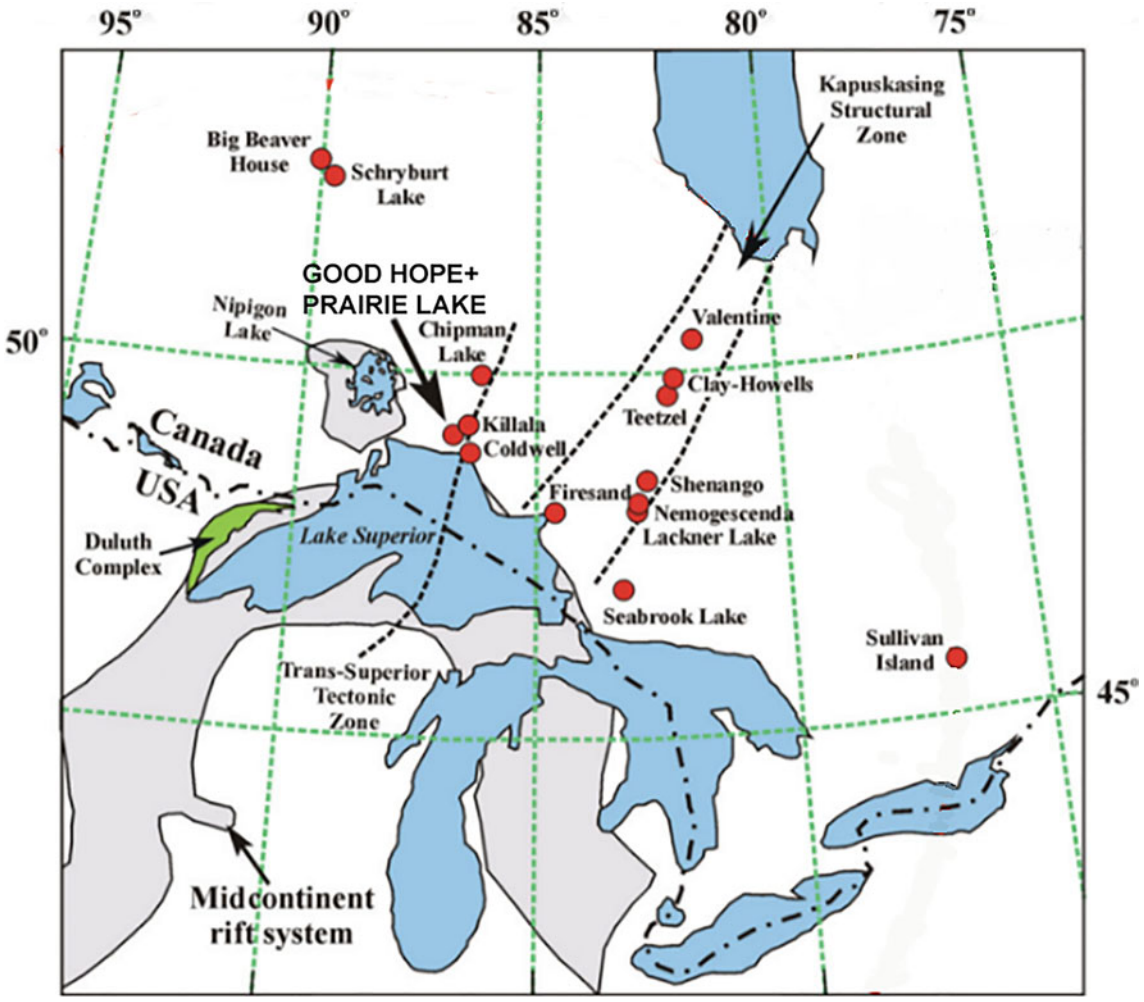

Fig. 1. Location of the Prairie Lake and Good Hope carbonatites together with those of other carbonatite and alkaline rock complexes in northwestern Ontario.

located adjacent to the Dead Horse Creek Road, northwest of the town of Marathon, ~26 km north of the shore of Lake Superior at 49°02'N, 86°43'W (Fig. 1). The carbonatites are emplaced in continental shield Archean gneisses of the Wawa Subprovince. The Prairie Lake complex has an emplacement age of ~1160 Ma (Rukhlov and Bell, 2010; Wu *et al.*, 2017). The age of the Good Hope carbonatite has yet to be determined but given the geological disposition is unlikely to differ from that of Prairie Lake.

The Prairie Lake complex (Fig. 2) consists in order of intrusion of: (1) biotite pyroxenites and coarse grained calcite carbonatites; (2) ijolite series rocks (urtite, ijolite, melteigite and hollaite); (3) malignites (*sensu* Mitchell and Platt, 1979); heterogeneous banded texturally diverse olivine phlogopite calcite carbonatites with numerous clasts and megaxenoliths of ijolite suite rocks, pyroxenites, phoscorite, pyroxene apatitite and wollastonite apatitite. Minor dolomite occurs only at the northern margins of the complex (Fig. 2). The complex has a well-defined magnetic signature (Sage, 1987) due to the presence of magnetite and has not been metamorphosed.

The Good Hope carbonatite is situated at the northwest margin of the Prairie Lake complex and adjacent to the heterogeneous banded carbonatites (Fig. 2). In contrast to the main complex there is no magnetic signature as magnetite is not present in these carbonatites. However, exploration work has established that there is a weak radiometric anomaly over parts of the carbonatite body. The absence of any magnetite anomaly and the paucity of outcrop is the reason that this carbonatite was not recognised previously. The geology of the Good Hope carbonatite has not yet been completely defined. Recent exploration by Plato Gold Corp. (www.platogold.com) has shown that occurrence encompasses an area of ~500 m × ~500 m, and has been proven by diamond drilling to extend to a minimum depth of 500 m.

The Good Hope carbonatite is a heterolithic breccia consisting of angular clasts of magnesio-arfvedsonite + potassium feldspar, potassium feldspar + phlogopite together with pyrochlore apatitite set in matrices consisting of dominant but diverse dolomite and ferrodolomite carbonatites, together with calcite carbonatites and lesser hydrothermal rare-earth-fluorocarbonate–fluorite–quartz–ferrodolomite carbonatite. The potassium-feldspar-bearing clasts are considered on textural and mineralogical grounds to be fragments of consanguineous intrusions, are not fenites, and will be described in a separate publication. The intrusion as a whole represents a complex of multiple generations of dolomite carbonatite intruded by younger calcite carbonatites. The Good Hope carbonatites have neither the texture nor the mineralogy of any of the Prairie Lake carbonatites. Notably absent are xenoliths or intrusions of ijolite-series rocks and malignites.

Mineralisation in the Good Hope carbonatite is represented principally by clasts of pyrochlore-bearing apatitite set in

https://doi.org/10.1180/mgm.2019.64 Published online by Cambridge University Press

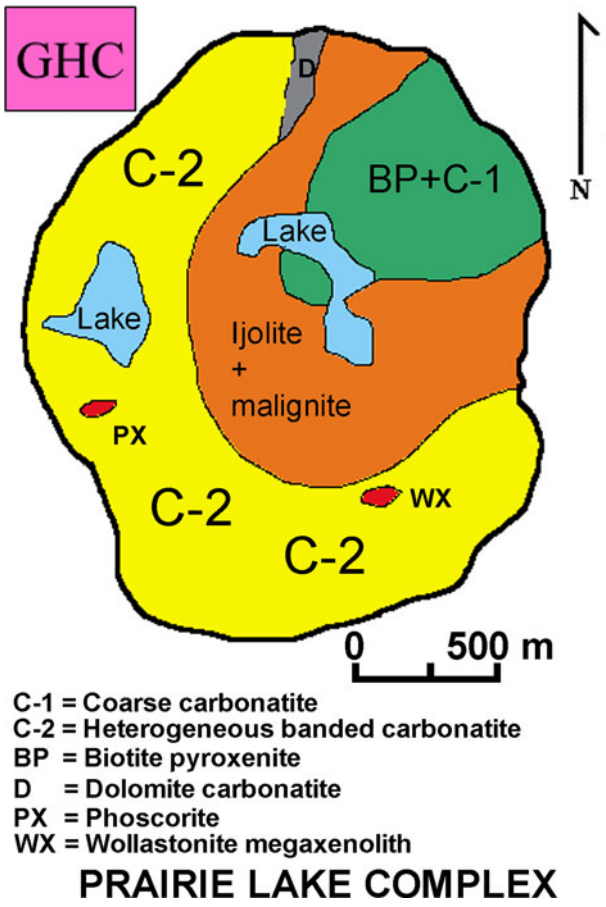

Fig. 2. General geology of the Prairie Lake Complex. The location of the Good Hope satellite carbonatite complex is located at the northwest margin of the complex and shown here, as there is no outcrop, as a magenta box representing the existing mineral deposit claims (GHC).

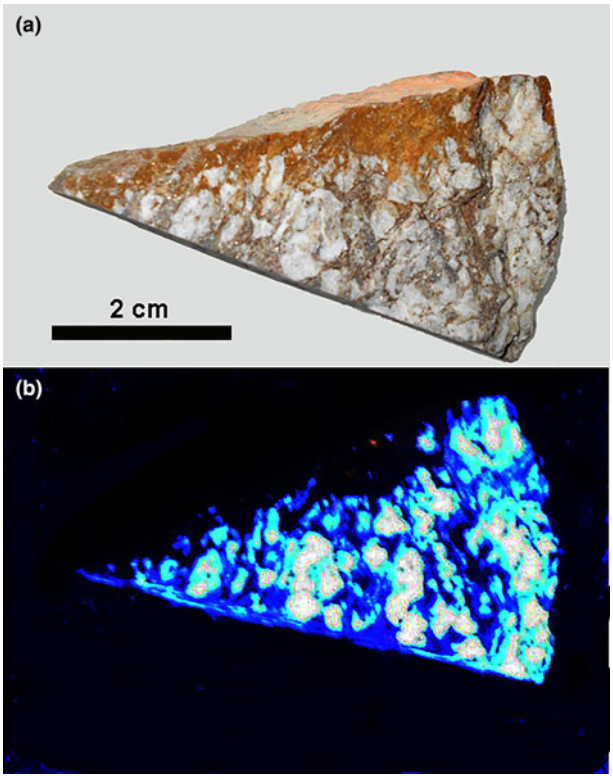

Fig. 3. Representative sample of Good Hope carbonatite illustrating; (*a*) white pyrochlore-apatitite clasts set in a brown ferrodolomite matrix; (*b*) clasts showing strong ultraviolet luminescence with blue cores and blue–green rims.

dolomite and ferrodolomite carbonatite matrices. Such carbonatites are consequently enriched in Nb. However, the distribution of the clasts is apparently random and diamond drilling to date has not established any continuous horizons of Nb-enriched carbonatite, nor encountered the undisrupted source of the apatitite clasts. In addition, disaggregation of apatitite clasts has led to the dissemination of pyrochlore in later intrusions of carbonatite which has also crystallised texturally- and compositionally-different primary pyrochlores. Hence, as a consequence of this heterogeneity, assessment of the Nb potential of this deposit is difficult without further definition drilling and large-scale bulk sampling. To-date diverse grab, channel and core samples have established Nb contents ranging from 0.1–1.63 wt.% Nb_2O_5, with 1 metre channel samples in an excavated pit ranging from 0.41–1.21 wt.% Nb_2O_5. Although an average grade has yet to be defined, it is apparent the Nb potential of this carbonatite is similar to, or exceeds, those of other primary niobium deposits in carbonatites which have been, or are being, exploited: Fen (0.5 wt.%); St Honoré (0.41 wt.%); Oka (0.45–0.66 wt.%); Panda Hill 0.43–0.87 wt.%; Elk Creek 0.67 wt.%) (see Mitchell, 2015).

Experimental methods

The compositions of apatite and pyrochlore were determined at Lakehead University by quantitative X-ray energy dispersive spectrometry (EDS) using a Hitachi SU–70 scanning electron microscope. X-ray spectra collected for 120 s with an accelerating voltage of 25 kV and beam current of 300 pA were processed using *AZtec* software (Oxford Instruments). Analytical standards were: apatite (P, Ca); $SrTiO_3$ (Sr, Ti); $ThNb_4O_{12}$ (Th, Nb); Mn-hortonolite (Mn, Fe, Mg and Si); jadeite (Na, Al), individual rare-earth orthophosphate glasses; Ta and U metals. The determination of the F content of apatite with a CaF_2 standard (collection time 250 s) is considered accurate (±2 wt.%) as there are no peak overlaps by O*K*α or Fe*K*α lines with the F*K*α line.

Trace-element data for apatite were determined on polished sections by laser ablation inductively coupled plasma mass spectrometry at the University of Manitoba using a 213 nm Nd-YAG New Wave laser connected to a Thermo Finnigan Element 2 sector-field mass spectrometer. Data were collected using spot analysis (55 μm) at a repetition rate of 5 Hz, ablation time of 50 s and energy density of 5.5 J/cm^2. The ablation was performed in argon and the rate of oxide production as measured by the ThO/Th ratio was set to 0.15%. The synthetic glass standard NIST SRM 610 was employed for instrument calibration and USGS BCR2G for quality control. The following isotopes were chosen for analysis: ^{29}Si; ^{32}S; ^{43}Ca; ^{55}Mn; ^{88}Sr; ^{89}Y; ^{137}Ba; ^{139}La; ^{140}Ce; ^{141}Pr; ^{143}Nd; ^{147}Sm; ^{151}Eu; ^{157}Gd; ^{159}Tb; ^{163}Dy; ^{165}Ho; ^{167}Er; ^{169}Tm; ^{172}Yb; ^{175}Lu and ^{232}Th. A Ca content of 55 wt.% CaO was used as an internal standard for all analyses as apatite in these clasts has near-stoichiometric fluorapatite composition (see below). Data reduction was undertaken online using *Iolite version 3* software (Hellstrom *et al.*, 2008).

https://doi.org/10.1180/mgm.2019.64 Published online by Cambridge University Press

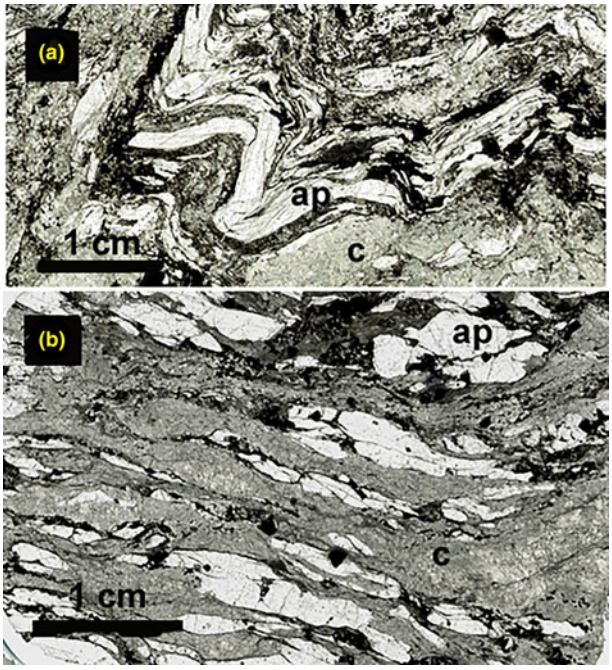

Fig. 4. Visible light scans of thin sections of Good Hope carbonatite illustrating: (*a*) folded bands of apatite prisms; (*b*) boudinaged apatitite clasts. Note that these carbonatites have *not* been subjected to metamorphism or regional tectonic deformation. (ap = apatitite; c = carbonate)

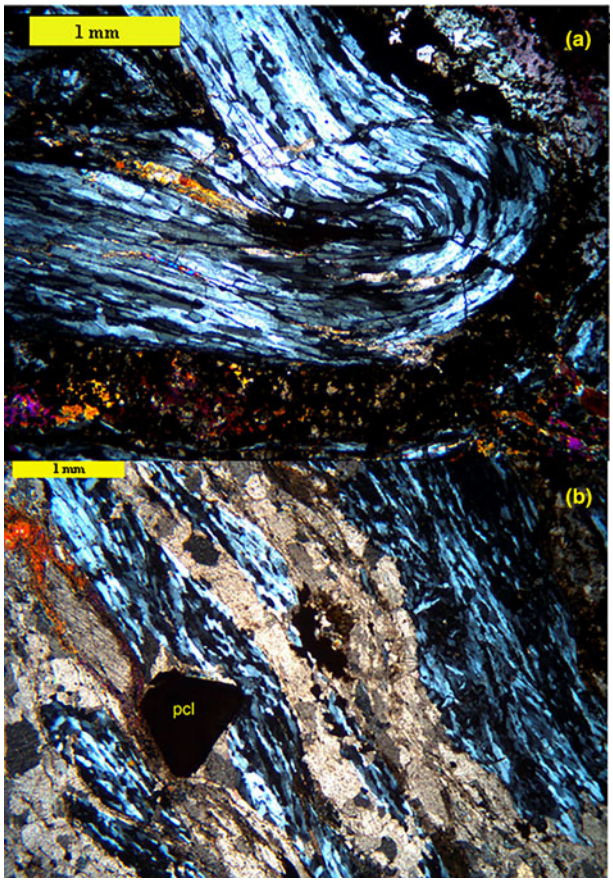

Fig. 5. Crossed polarised light images of: (*a*) band of 'folded' apatite prisms illustrating the subparallel orientation of the prism axes and the anisotropic heterogeneity: (*b*) crossed polarised light image of deformed and elongated apatitite schlieren occurring as sub-parallel bands in a carbonate matrix with a large opaque pyrochlore (pcl) crystal.

Pyrochlore apatitite

Macroscopically, the apatitite clasts are typically irregular in shape and range in size from millimetres to centimetres (typically <2 cm; but up to 5 cm). A representative sample of mineralised carbonatite consisting of angular white apatitite clasts set in a brown ferrodolomite host is illustrated in Fig. 3*a*. The clasts are fine grained and their internal texture is not evident in hand samples. The apatitite clasts fluoresce strongly in ultraviolet light (Fig. 3*b*); a feature which permits the easy recognition of potentially Nb-rich apatitite clasts in diamond drill core samples.

Apatitites – texture and mineralogy

The apatitite clasts exhibit diverse textures ranging from apparently folded clasts (Fig. 4*a*; Fig. 5*a*) through elongated and boudinaged types (Fig. 4*b*) to schlieren-like (Fig. 5*b*) sub-parallel varieties. The clasts consist of apatite prisms (Fig. 6*a*) which range in size from ~100–500 μm × 10–25 μm. In some instances grain boundaries are highlighted by thin films of brown Fe-oxides/hydroxides or extremely fine-grained amorphous mixtures of unidentifiable minerals containing C, Mg, Si, S, Cl, Ca, Fe and Cu. Although individual prisms typically exhibit undulose extinction there is no common optical orientation within a given clast (Fig. 6*b*). In some of the smaller clasts, and at the terminations of boudinaged clasts, the apatites are rarely coarsened into anhedral grains with uniform extinction. Allotriomorphic granular textures typical of sub-solidus coarsened cumulates are not present.

The apatite prisms have no internal mineral or fluid inclusions. The pyrochlores present in the clasts have apparently crystallised prior to the prismatic apatite as they lack prismatic apatite inclusions (see below). Deflection of apatite prisms around pyrochlores is present but not common and the orientation of prisms are typically not disturbed by the presence of pyrochlore.

The apatite in addition to the strong blue–green ultraviolet fluorescence exhibits cathodoluminescence (CL). Figure 7*a* illustrates a hot cathode CL image of apatite in a portion of a folded clast and shows the presence of green luminescent cores mantled by thin blue–green rims. Figure 7*b* illustrates a cold cathode CL image of apatite which exhibits the common blue CL of primary apatite occurring in carbonatites (Mitchell, 2014). The marginal CL evident in the ultraviolet fluorescence and hot cathode CL is present but not well defined. The CL spectrum (Fig. 7*c*) is dominated by complex Sm, Pr and Dy emission (550–650 nm) together with a broad blue–green band (400–500 nm) attributed to Eu or Ce, and a weak Nd emission in the infra-red (850–900 nm). Mitchell (2014) has noted that the CL spectra of apatite from carbonatites consist of two groups: (1) those with a broad 400–500 nm band in the blue region of the spectrum (Verity, Howard Creek, Big Beaver House); and (2) those lacking this band (Fen, Oka, Cargill). The reasons for this dichotomy have not yet been established. Good Hope apatite belongs to group 1, whereas apatite derived from Prairie Lake heterogeneous carbonatites belongs to group 2 (Mitchell, 2014).

Carbonatites containing folded apatitites of the type found at Good Hope have not been described previously. The folding, boudinage and schlieren textures are not due to external tectonic deformation by events subsequent to crystallisation of the

https://doi.org/10.1180/mgm.2019.64 Published online by Cambridge University Press

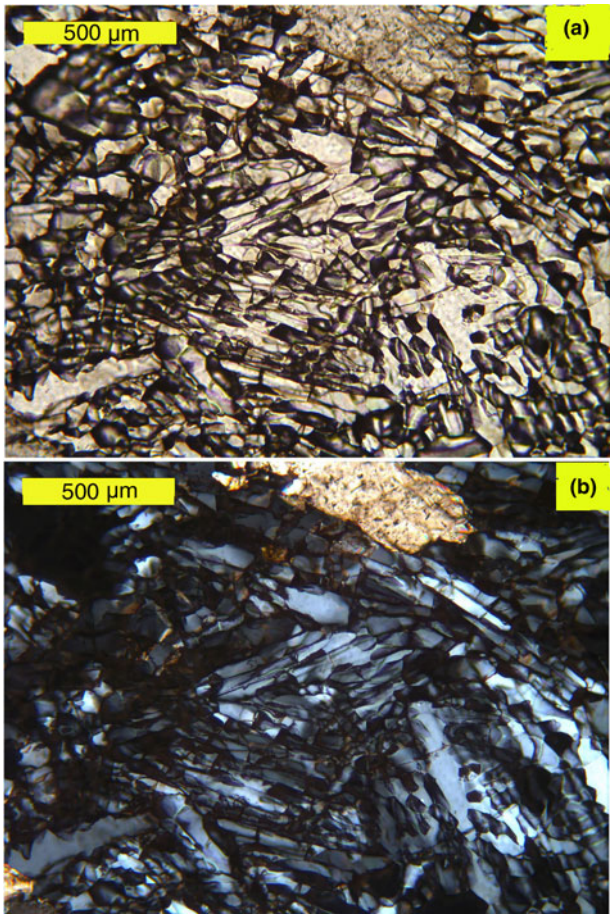

Fig. 6. Typical texture of apatite in the apatitite clasts in: (*a*) plane polarised light; and (*b*) crossed polarised light.

carbonatites, as neither Good Hope nor Prairie Lake have been metamorphosed and are emplaced in a stable craton. The folds shown in Fig. 4*a* are not analogous to folded apatite described by Chakhmouradian *et al.* (2015) from the Aley carbonatite as this intrusion, in common with other carbonatites in the British Columbian Cordillera, have been subjected to metamorphism and tectonic deformation subsequent to their emplacement (Mitchell *et al.*, 2017).

Folded apatitite similar to the Good Hope clasts are apparently rare as most accumulations of apatite in carbonatites consist of subhedral crystals with allotriomorpic granular rather than prismatic textures, although when present prisms tend to be large (0.1–15 mm) isolated euhedral to subhedral crystals. An apatite carbonatite with folded bands of apatite has been noted from the Ngualla carbonatite (Tanzania) by Witt *et al.* (2019). This carbonatite has not been metamorphosed or deformed tectonically. Unfortunately, only a macroscopic description was presented by Witt *et al.* (2019) without accompanying textural or mineralogical data. Deformed apatitite clasts have been recognised (this work) from the St. Honoré (Québec) carbonatite which are analogous to the Good Hope folded clasts. In this example (Supplementary Fig. S1, see below) apatite prisms plus pyrochlore are deflected around large magnetite crystals. Clearly, on the basis of their texture prismatic apatitite clasts must have a different genesis and/or subsolidus re-equilibration history to granular types (see below).

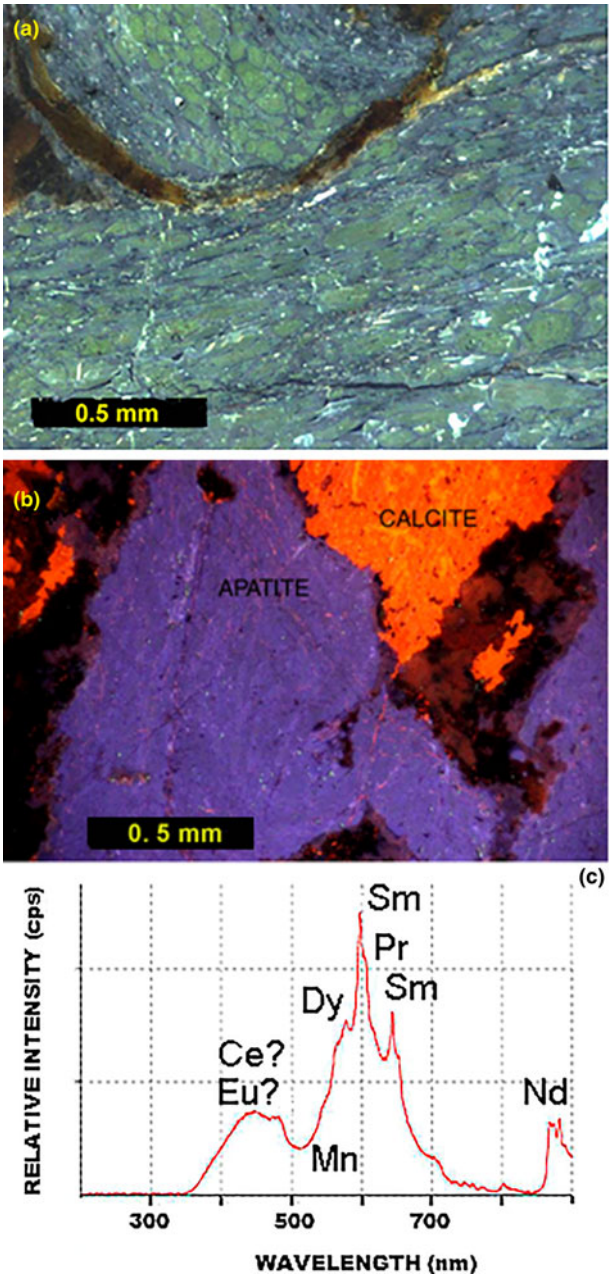

Fig. 7. (*a*) Hot cathode luminescence image of folded apatite prisms illustrating green cores and thin blue green margins; (*b*) cold cathode luminescence image of apatite in apatitite clasts showing the typical blue CL of carbonatite apatite; (*c*) CL spectrum of apatite (see text for discussion).

Apatite – composition

The apatite-group mineral comprising the apatitite clasts is close in composition (3.6–3.8 wt.% F; 41.2–41.5 wt.% P_2O_5; 54.9–55.0 wt.% CaO) to ideal $Ca_5(PO_4)_3F$ and is thus fluorapatite. The only minor element detectable by quantitative EDS is Sr (~0.9–1.1 wt.% SrO). Compositional zoning is not evident in back-scattered electron images.

Of the trace elements (ppm) present the most notable are: Si 108–572; Mn 79–396; Sr 7030–13,000; Y 139–439; Ba 25–59; Th 3.8–17; La 589–1280; Ce 1830–3940; Pr 262–571; Nd 1450–2740; Yb 5.2–12. The full data set is given in Supplementary Table S1 (see below). Representative data, only for apatite cores

https://doi.org/10.1180/mgm.2019.64 Published online by Cambridge University Press

Table 1. Representative trace-element compositions (ppm) of apatite.*

	VAL2	VAL4A	337	540	PX-A	W-A
Si	247	281	291	248	3510	4490
Mn	342	173	336	294		
Sr	13,000	9650	8620	8710	7470	9380
Y	212	239	194	197	484	408
Ba	48	25	36	34	22	13
La	1280	915	1146	831	2170	2870
Ce	3940	2680	3230	2420	5380	6240
Pr	571	292	432	383	731	720
Nd	2740	1657	2180	2210	2910	2999
Sm	287	269	235	243	500	422
Eu	83	81	69	69	129	100
Gd	167	183	159	152	360	266
Tb	21	18	21	18	37	25
Dy	77	87	71	71	165	103
Ho	11	11	10	9	24	15
Er	24	18	18	19	44	28
Tm	1.9	1.8	1.7	1.6	4.2	2.7
Yb	8.8	5.4	6.9	7.9	18	11
Lu	0.23	0.17	0.19	0.11	2.2	1.3
Th	6.4	6.8	17	3.7		

*Good Hope: VAL2, VAL4A and 337 prismatic apatite; 540 coarse grained anhedral apatite. Prairie Lake: PX-A apatite in pyroxene apatitite; W-A apatite in wollastonite apatitite. Blanks indicate below limit of detection.

are given in Table 1, as the rims evident in CL are too small for analysis with the analytical system employed. Figure 8 illustrates chondrite-normalised (CN) rare earth element (*REE*) distribution patterns for Good Hope apatite. Although the patterns show a general depletion in *REE* abundance from La–Lu two distinct segments are evident with an inflection at Nd–Sm: a relatively flat segment from La–Nd; and a smoothly decreasing segment from Sm–Yb. The former is a consequence of these apatites having relatively low La/Nd_{CN} ratios (0.73–1.14) in comparison to apatite from other carbonatites which exhibit smooth *REE* distribution patterns from La–Yb [e.g. Alnö 1.8–2.9; Fen; 1.80; Jacupiranga 1.58; Hornig-Kjarsgaard (1998); Kaiserstuhl 2.94–4.04; Wang *et al.* (2014); Belaya Zima 1.53–1.77; Doroshkevich *et al.* (2017)]. These data are interpreted to imply that the Good Hope apatites are relatively depleted in La, Ce, Pr and Nd. Another notable difference is their paucity in Si (108–572 ppm) compared to other carbonatite apatite [2000–2288 ppm Kaiserstuhl; 560–1494 ppm; Wang *et al.* (2014); Doroshkevich *et al.* (2017)].

Anhedral single crystals of apatite in the Prairie Lake heterogeneous carbonatites, in marked contrast to Good Hope apatite, in common with many other carbonatite apatites (Hornig-Kjarsgaard, 1998; Wang *et al.*, 2014; Doroshkevich *et al.*, 2017), exhibits smooth chondrite-normalised *REE* distribution patterns

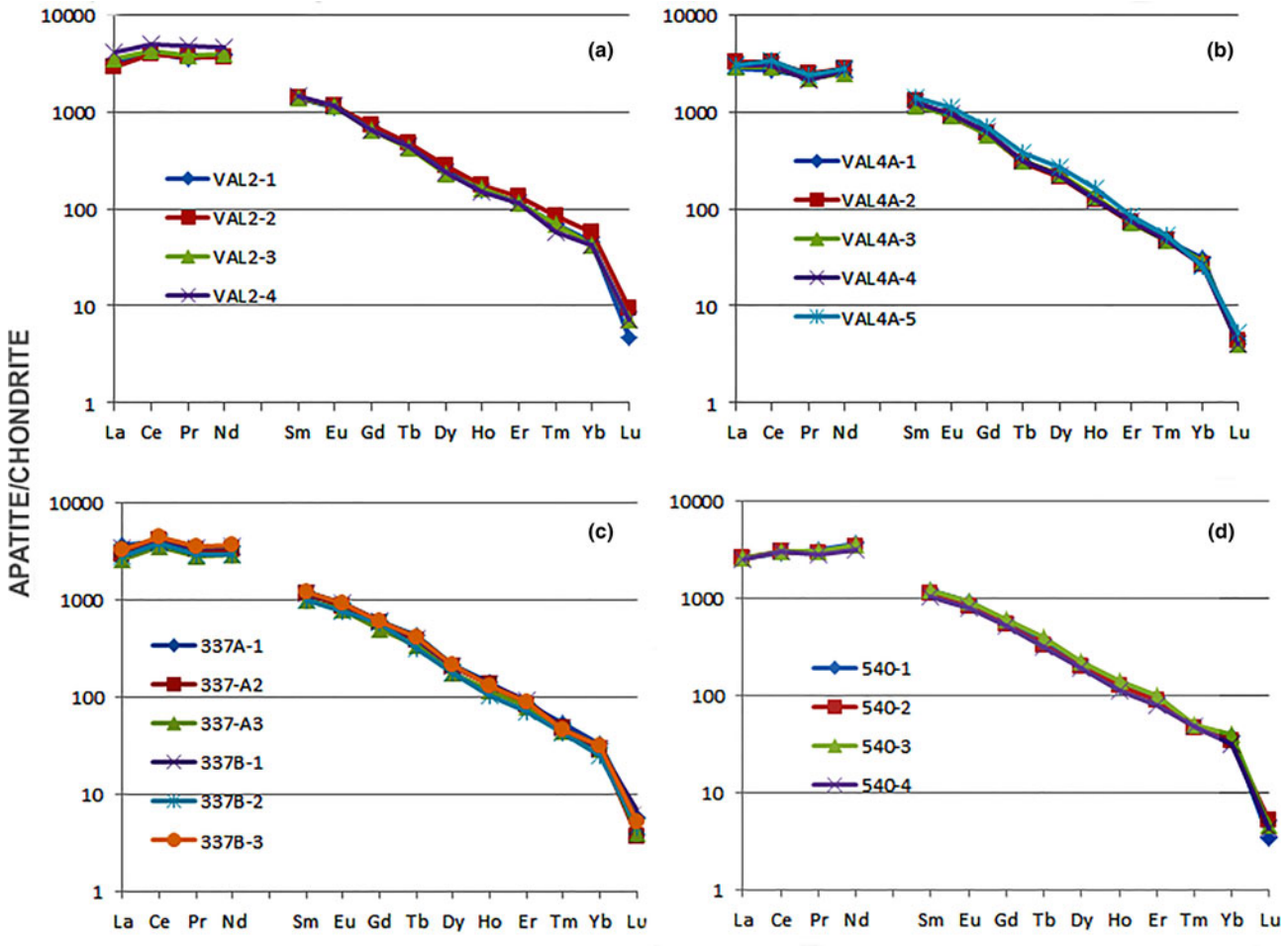

Fig. 8. Chondrite-normalised (Boynton, 1985) *REE* distribution patterns of apatite in four different apatitite clasts. Samples (*a*) VAL2 and (*b*) VAL4A are from near-surface exploration pits. Data for VAL2 are for the folded clast shown in Figs 3 and 8. Samples (*c*) 337 and (*d*) 540 are different levels (depth in metres) from 60° and 50° inclined drill cores in the complex. These data show that *REE* distributions are very similar regardless of location in the complex.

https://doi.org/10.1180/mgm.2019.64 Published online by Cambridge University Press

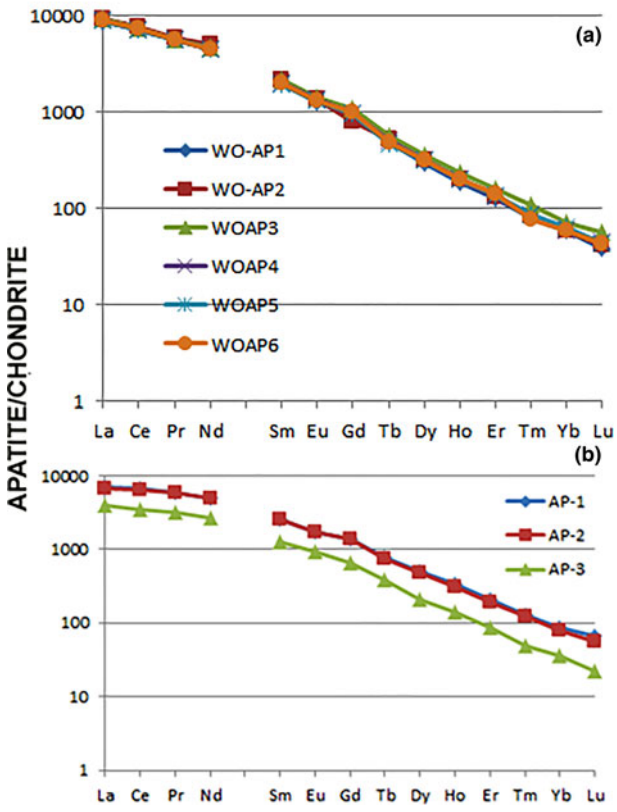

Fig. 9. Chondrite-normalised (Boynton, 1985) *REE* distribution patterns of apatite from (*a*) wollastonite apatitite and (*b*) pyroxene apatitite xenoliths in the Prairie Lake heterogeneous carbonatites. Note that these apatite do not exhibit the La–Nd depletion evident in the Good Hope apatites illustrated in Fig. 8.

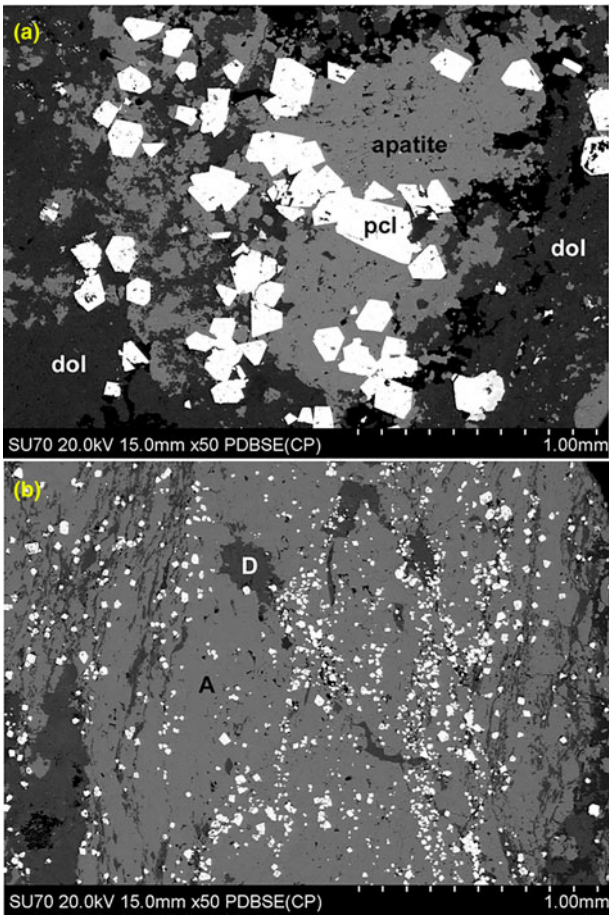

Fig. 10. Back-scattered electron images at the same scale of pyrochlore (white) enclosed in apatite in different apatitite clasts illustrating the extremely wide range in size of the crystals. Note that the majority of pyrochlores are single euhedral crystals. (A = apatite; pcl = pyrochlore; D and dol = dolomite). Scale bar = 1 mm with 100 μm divisions.

with La/Nd_{CN} 1.26–2.0 (see fig. 3 in Wu *et al.*, 2017). Apatite in allotriomorphic granular apatitite cumulates occurring as mega-xenoliths in the Prairie Lake heterogeneous carbonatite exhibit smooth La–Lu distribution patterns with La/Nd_{CN} ratios ranging from 1.36–1.53 and 1.85–2.01 for pyroxene apatitite and wollastonite apatitite, respectively (Fig. 9). These data further emphasise the unusual textural and geochemical character of the Good Hope apatite relative to that in the main carbonatites of the Prairie Lake complex.

Pyrochlore paragenesis

Pyrochlore is the only primary Nb-bearing mineral in the apatitite clasts. The pyrochlore occurs primarily as euhedral single crystals which exhibit a wide range in size from ~50 μm to 1 mm, with the majority ranging from 300–600 μm (Figs 5, 10–11). Large aggregations of pyrochlore with allotriomorphic granular textures are not present, although clusters of two to three intergrown euhedral-to-subhedral 30–100 μm crystals are relatively common. The pyrochlores exhibit a very wide range of characters depending on: the abundance of inclusions of apatite and calcite; the extent of compositional zoning; and replacement by other Nb-bearing minerals. Note that apatites included in pyrochlore occurs as small (<15 μm) inclusions of irregular amoeboid shape and prismatic apatite is rarely present: both these and anhedral calcite are possibly secondary inclusions.

The majority of the pyrochlores show only minor resorption although some crystals appear to have been broken prior to incorporation in their host apatitite clasts (Fig. 11*a*). Euhedral and broken single crystals can be found with a given clast. Pyrochlores are also common as single crystals disseminated in the ferrodolomite and late-stage hydrothermal quartz-bearing carbonatites. Some of these pyrochlores are derived from the disaggregation of apatitite clasts whereas others are primary minerals which have apparently crystallised from the diverse later intruded carbonatites. Such pyrochlores are commonly smaller than those in the apatite clasts, exhibit complex oscillatory compositional zoning and can host inclusions of quartz or magnesio-arfvedsonite. Description of the paragenesis and composition of all pyrochlores in the Good Hope carbonatites is beyond the scope of this work, and will be the subject of a subsequent manuscript.

The pyrochlores in the apatitite clasts exhibit many similar textural and compositional characteristics although these differ between individual clasts (Figs 11,12). All pyrochlores exhibit compositional zoning in back-scattered electron images. This can range from a few very thin bands of higher average atomic number in an otherwise uniform crystal (Fig. 12*a*) and more rarely to complex zoning from an irregular high average atomic number core to multiple growth bands of differing composition (Fig. 12*b*). The pyrochlores range from essentially alteration-poor varieties to those with minor or near complete replacement by fine-grained (<20 μm) anhedral crystals of either columbite-(Fe) (Fig. 12*c*) and/or fersmite (Fig.12*c*), with some crystals replaced by both

https://doi.org/10.1180/mgm.2019.64 Published online by Cambridge University Press

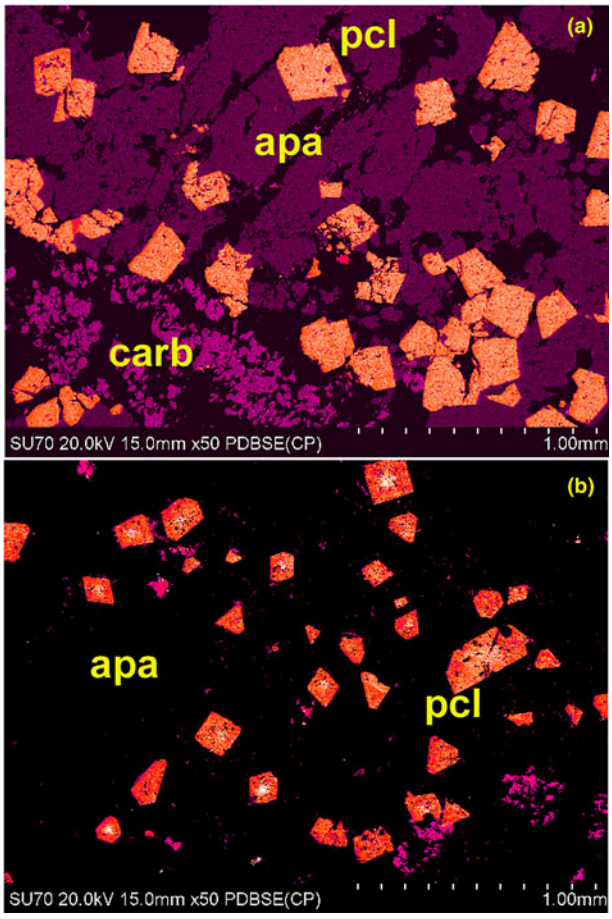

Fig. 11. False-colour back-scattered electron images of pyrochlores in two different apatitite clasts demonstrating that individual clasts differ with respect to the size and compositional zoning of the pyrochlores. (*a*) Na–Ca pyrochlores with columbite-(Fe); (*b*) pyrochlores with *A*-site deficient Sr, Ba and Fe enriched cores (white) and Na–Ca pyrochlore margins. (pcl = pyrochlore; apa = apatite; carb = carbonates). Scale bar = 1 mm with 100 μm divisions.

minerals in fine-grained intergrowths. Columbite-(Fe) is Ti- and V-bearing with up to 6 wt.% TiO_2 and 3.5 wt.% V_2O_5. Fersmite is near stoichiometric $CaNb_2O_6$ with minor TiO_2 (2–3 wt.%) and FeO_T 0.6–3.2 wt.%). Note that discrete crystals of these niobates are not present in the apatitites or the associated carbonatites.

Pyrochlore composition

Pyrochlore-group compounds have the ideal structural formula $A_2B_2O_6Z$. In carbonatites pyrochlores are not stoichiometric and contain cation vacancies (Atencio *et al.*, 2010); typical compositions are expressed as $[(Ca,Na,Sr,Ba,Ce,U^{4+})_{2-x}(Nb,Ti,Ta,Fe^{3+})_2O_6(OH,F)_{1-y}\cdot zH_2O]$. Hydroxyl anions and H_2O cannot be analysed by EDS and F determination is not exact due to significant overlaps of the F*K*α peak with diverse low-energy X-ray peaks (particularly Fe*L*α). Pyrochlore compositions obtained by both wavelength-dispersive and energy-dispersive electron beam methods are generally expressed on a volatile-free basis with the number of *B*-site cations fixed at 2.0 (Hogarth *et al.*, 2000), as unlike *A*-site cations these are considered not to be subject to leaching during weathering and/or hydrothermal activity (Lumpkin and Ewing, 1995). The *A*-site deficiency is commonly used as a measure of alteration or metamictisation (Nasraoui and Bilal, 2000; Zurevinski and Mitchell, 2004). Representative compositions of Good Hope pyrochlores in apatitite clasts are given in Table 2. All of the pyrochlores in the Good Hope apatitites are poor in Ti and Ta. As Nb > Ti >> Ta (atoms per formula unit) they are classified as pyrochlore *sensu stricto* (Hogarth, 1977; Atencio *et al.*, 2010).

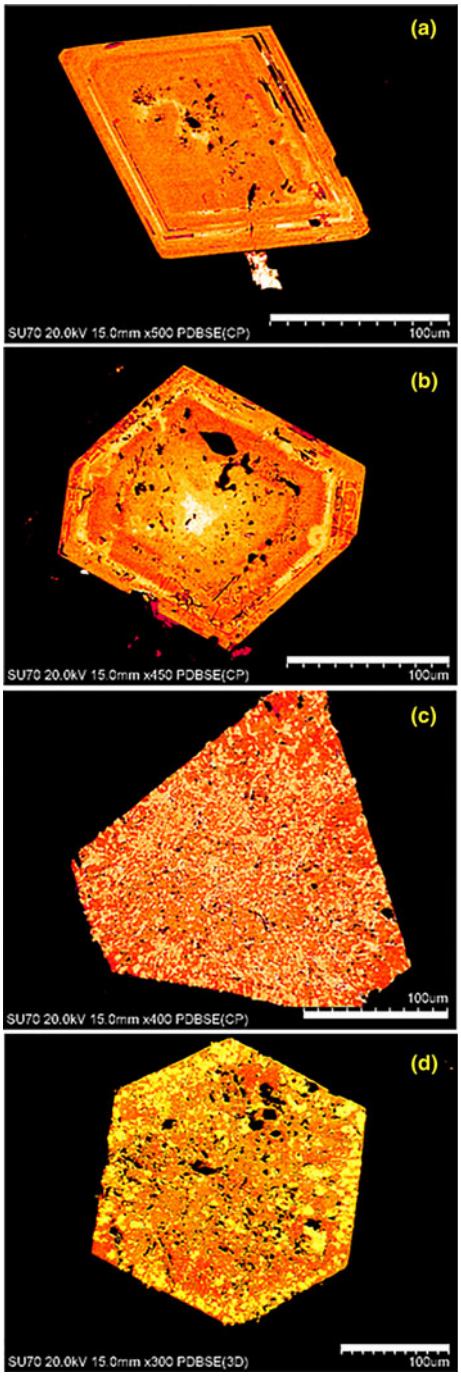

Fig. 12. False-colour back-scattered electron images illustrating the range of compositional zoning occurring in Good Hope pyrochlores from apatitite clasts. (*a*) Relatively uniform Na–Ca pyrochlore with thin oscillatory zoning resulting from Sr, Ba and Fe enrichment; (*b*) pyrochlore with an *A*-site deficient Sr, Ba and Fe enriched core (white) and zones of Na–Ca pyrochlore (orange) and Sr–Ba–Fe pyrochlore (yellow) margins; (*c*) small anhedral columbite-(Fe) crystals (yellow) replacing Na–Ca pyrochlore (orange); (*d*) anhedral fersmite (yellow) replacing Na–Ca pyrochlore (orange). Scale bar indicates 100 μm.

https://doi.org/10.1180/mgm.2019.64 Published online by Cambridge University Press

Table 2. Representative compositions (wt.%) of pyrochlore.*

	1	2	3	4	5	6	7	8
Wt.%								
Na_2O	7.19	7.98	7.17	4.87	3.97	1.37	1.89	2.22
SiO_2				1.22	0.46	2.16	1.85	2.77
CaO	16.28	15.85	15.76	11.22	12.08	10.46	10.77	8.89
TiO_2	3.31	4.17	3.94	2.98	3.16	2.33	2.21	5.02
Fe_2O_3				1.85	1.40	3.63	2.66	2.75
SrO	0.76	1.06	1.93	6.75	4.06	7.46	6.95	9.57
Nb_2O_5	71.40	68.52	70.08	64.36	67.16	64.41	65.53	57.59
BaO		0.51		1.57	0.72	2.77	2.59	3.31
Ta_2O_5				0.87				1.56
UO_2				0.46		1.06	1.15	1.82
Σ	98.94	98.09	98.88	96.15	93.01	96.65	95.50	95.50
Structural formulae calculated on the basis of 2 *B*-site cations								
Na	0.802	0.907	0.802	0.552	0.447	0.145	0.209	0.245
Si				0.071	0.027	0.118	0.105	0.158
Ca	1.003	0.996	0.975	0.703	0.756	0.614	0.657	0.543
Ti	0.143	0.184	0.171	0.131	0.139	0.137	0.095	0.215
Fe				0.081	0.062	0.150	0.114	0.118
Sr	0.025	0.036	0.065	0.229	0.137	0.237	0.229	0.316
Nb	1.857	1.816	1.829	1.702	1.773	1.595	1.686	1.485
Ba		0.012		0.036	0.016	0.059	0.058	0.074
Ta				0.014				0.024
U				0.006		0.013	0.015	0.023
Σ_{cat}	3.831	3.950	3.842	3.527	3.359	3.069	3.167	3.202
A site	1.831	1.950	1.842	1.527	1.359	1.069	1.167	1.202
Σ*A*	0.169	0.050	0.158	0.473	0.641	0.931	0.833	0.798

*Σ_{cat} = total cations; *A* site = total cations in this site; Σ*A* = *A*-site deficiency. Elements not detected at <0.4 wt.% oxide are: Mg; Al; Cl; Mn; *REE*; Pb. Blanks in the table indicate not detected.

Typically the commonest, earliest forming and least replaced pyrochlores (Fig. 12*a*) are Na–Ca pyrochlore that is poor in Sr and has only minor (5–20%) *A*-site deficiency (Table 2, comps. 1–3). Thin oscillatory bands of higher average atomic number are present in some crystals which have increased Sr and Ba contents and lower Na (Table 2, comps. 4–5), but are not otherwise markedly different. Less commonly, pyrochlores exhibit strong compositional zoning (Fig. 12*b*) with typically irregular cores of Na–Ca depleted material with high average atomic number consisting of *A*-site deficient (>50%) pyrochlore enriched in Sr, Ba, Fe, Si and U (Table 2; comp. 6–8). These cores are typically overgrown by, or are gradational into, Na–Ca pyrochlores without *A*-site deficiency. The example shown in Fig. 12*b* illustrates further syntaxial overgrowth of Sr-rich pyrochlore followed by Na–Ca pyrochlore.

From the above textural and compositional data it is apparent that many pyrochlores have had a complex evolutionary history and that more than one generation of pyrochlore is present. The suite has some similarities to pyrochlore populations in other carbonatites in which U–Ta-enriched pyrochlore of irregular habit is enclosed in oscillatory zoned pyrochlore (Walter *et al.*, 2018; Lee *et al.*, 2006; Zurevinski and Mitchell, 2004; Hogarth *et al.*, 2000; Chakhmouradian and Zaitsev, 1999). However, note that extensively oscillatory zoned pyrochlores of the type illustrated in figure 2C of Hogarth *et al.*, 2000) or figures 2A and 2C of Walter *et al.* (2018) are not found at Good Hope.

Walter *et al.* (2018) and Lee *et al.* (2006) have suggested that the U–Ta enriched pyrochlore cores in Kaiserstuhl and Sokli carbonatites are resorbed xenocrysts which did not crystallise from the magma which crystallised oscillatory zoned pyrochlore overgrowths. Similar Good Hope pyrochlores might have had such an origin but they cannot be linked to any pyrochlores crystallising from co-genetic silicate magmas, as there is no geological evidence for the presence of such magmas i.e. xenoliths, consanguineous pyrochlore-bearing intrusions, interaction with, or derivation from, the main Prairie Lake occurrences of ijolites and carbonatites. In addition, the Good Hope Sr–Ba–Fe–U enriched cores are notably poor in U and Ta (<2 wt.% UO_2; <1 wt.% Ta_2O_5) relative to Kaiserstuhl and Sokli types (>20 wt.% UO_2; >9 wt.% Ta_2O_5). An alternative explanation for Ta, and by analogy Sr, Ba, Fe and U, enrichment in early crystallising pyrochlores has been suggested by Kjarsgaard and Mitchell (2008), who note that Ta-rich pyrochlores are F poor and Ta poor whereas Na–Ca pyrochlores are F rich. Although quantitative compositional data for F are not available for Good Hope pyrochlores, semi-quantitative data suggest that the strongly *A*-site deficient pyrochlores have lower F (<3 wt.% F) contents than Na–Ca pyrochlores (<4 wt.% F) Thus, it is suggested that variations of F fugacity in the melt can also lead to the crystallisation of different varieties of pyrochlore.

Currently, oscillatory zoning of pyrochlores is considered to have magmatic origins (Hogarth *et al.*, 2000), and to be originating from supersaturation of magma with mineral end-members of different solubilities. Oscillatory zoning is considered to occur in undisturbed environments, whereas homogeneous crystals form in turbulent conditions. Thus, crystals exhibiting both homogeneous regions and oscillatory zoning might reflect either (or both) *in situ* growth with repeated changes in magma rheology from turbulence to quiescence or transport of growing crystals from one rheological regime to another.

The observations suggest the Good Hope pyrochlore suite has diverse origins with some pyrochlores formed by incorporation of Sr, Ba, Fe and U-rich pyrochlore into a magma (of higher F fugacity?) crystallising mainly homogeneous Na–Ca pyrochlore and/or oscillatory zoned pyrochlore with alternating conditions of turbulence and quiescence. Thus, pyrochlores with, or lacking, enriched cores can coexist with homogeneous and/or oscillatory zoned types. Many, but not all pyrochlores were then subject to alteration and replacement by fersmite and columbite-(Fe), with some altered crystals being returned to environments where homogeneous overgrowth of Na–Ca pyrochlore were resumed. Overall the suite represents growth under diverse rheological conditions and is undoubtedly a consequence of magma mixing.

Genesis of the pyrochlore apatitites

Experimental studies of Nb-bearing haplocarbonatites have a bearing on the origins of the pyrochlore apatitites as these indicate that pyrochlore can be the initial crystallising phase over a wide range of bulk compositions and temperatures (Mitchell, 2004; Jago and Gittins, 1993). For example, Mitchell and Kjarsgaard (2004) have shown that in the system $NaNbO_3$–$CaCO_3$–CaF_2 there is a large high temperature (>900°C) pyrochlore liquidus phase field for bulk compositions with up to 40 wt.% $NaNbO_3$ along the join $[CaCO_3)_{60}(CaF_2)_{40}]$–$NaNbO_3$.

Textural relationships between pyrochlore and apatite indicate that the pyrochlores formed prior to incorporation in apatite matrices and undoubtedly were, in accord with the experimental studies, the primary liquidus phase in their parental magma. If this magma was held at diverse temperatures within the liquidus field of pyrochlore it is possible that a suspension of isolated crystals would be formed that experienced changes in composition and rheology giving rise to the observed diverse types of compositional zoning but without the crystals sinking rapidly to form cumulates. The pyrochlores cannot represent a disrupted annealed cumulate as

https://doi.org/10.1180/mgm.2019.64 Published online by Cambridge University Press

fragmentation of allotriomorphic granular clasts would release pyrochlores of different morphology to those observed in the apatitite clasts. It is apparent that cooling of the magma parental to the pyrochlores did not reach either an apatite–pyrochlore or a calcite–pyrochlore cotectic. Thus, to explain the observed association with apatite this diverse assemblage of pyrochlore crystals must eventually have been transported as individual crystals to an environment where apatite was crystallising and accumulating.

Unfortunately there are no experimental studies of haplocarbonatite systems involving both niobium and phosphorus. The only investigation of P-bearing haplocarbonatite is that of Wyllie and Biggar (1966). This study showed that apatite has very limited solubility in haplocarbonatite magmas and that undoubtedly it can be the initial liquidus phase over a wide range of compositions and temperature at 1 kb pressure. These observations combined with the prediction above that pyrochlore can also be an initial crystallising phase suggest that either pyrochlore or apatite can be an initial liquidus phase depending on the bulk composition of the magma. It also follows that with magma crystallisation, bulk compositions should reach a cotectic involving both phases. However, the observed textures of the apatitite clasts suggest that both minerals crystallised independently, with pyrochlore in a relatively quiescent regime and no crystal settling to form cumulates, in contrast to the small prismatic aligned apatite crystals with textures suggestive of a transported assemblage in a turbulent environment.

Conclusions

On the basis of the above discussion, a preliminary hypothesis for the formation of the pyrochlore-apatitite clasts is: (1) crystallisation of pyrochlore as the primary liquidus phase from an unidentified magma with formation of single crystals exhibiting diverse compositional zoning due to variations in solubility, magma rheology and volatile fugacities; alteration and replacement of pyrochlore by fersmite and columbite-(Fe); (2) rapid crystallisation of apatite in a different and also unidentified magma as an initial liquidus phase; concentration of apatite as swarms of small prismatic crystals by magmatic currents; (3) magma mixing with transport of apatite into the pyrochlore-bearing magma by turbulence with mechanical incorporation of pyrochlores in apatite; (4) lithification of the apatite plus pyrochlore as pyrochlore apatitite; and finally disruption of the apatitite 'pseudocumulate' by later intrusions of carbonatite with formation of apatitite clasts in ferrodolomite and calcite carbonatite hosts.

Overall the genesis of the apatitite clasts is considered to be one of magma mixing and is thus a rheological process rather than one of simple differentiation of a single parental magma. Unfortunately, the character of the parental magmas and the geological location of unfragmented apatitites at depth in the Good Hope intrusion as yet remains unknown. One objective of current exploration at the Good Hope Nb property is to locate undisrupted apatitites as these could form a significant high-grade Nb deposit

Acknowledgements. This study is supported by Plato Gold Corporation, Almaz Petrology, The Wahl Group, and Lakehead University. Sam Broom-Fendley and two anonymous reviewers are thanked for comments on the initial draft of this paper. Stuart Mills and Helen Kerbey are thanked for the Editorial and Production aspects of the publication of this work.

Supplementary material. To view supplementary material for this article, please visit https://doi.org/10.1180/mgm.2019.64

References

Atencio D., Andrade M.B., Christy A.G., Gieré R. and Katashov P.M. (2010) The pyrochlore supergroup of minerals: nomenclature. *The Canadian Mineralogist*, **48**, 673–698.

Boynton W.V. (1985) Cosmochemistry of the rare earth elements: Meteorite studies. Pp. 115–152 in *Rare Earth Element Geochemistry* (P. Henderson, editor). Developments in Geochemistry 2, Elsevier, Amsterdam.

Chakhmouradian A.R. and Zaitsev A.N. (1999) Calcite-amphibole-clinopyroxene rock from the Afrikanda Complex, Kola Peninsula, Russia: mineralogy and a possible link to carbonatites: I, oxide minerals. *The Canadian Mineralogist*, **37**, 177–198.

Chakhmouradian A.R., Reguir E.P., Kressall, R.D., Crozier J., Pisiak L.K., Sidhu R. and Yang P. (2015) Carbonatite-hosted niobium deposit at Aley, northern British Columbia (Canada): Mineralogy, geochemistry and petrogenesis. *Ore Geology Reviews*, **64**, 642–666.

Doroshkevich A.G., Veksler I.V., Klemd R., Khromova E.A. and Izbrodin I.A. (2017) Trace element composition of minerals and rocks in the Belaya Zima carbonatite complex (Russia): implications for the mechanisms of magma evolution and carbonatite formation. *Lithos*, **284–285**, 91–108.

Hellstrom J., Paton C., Woodhead J.D. and Hergt J.M. (2008) Iolite: software for spatially resolved LA-(quad and MC) ICPMS analysis. P. 343 in: *Laser Ablation ICP–MS in the Earth Sciences: Current Practices and Outstanding Issues* (P. Sylvester, editor). Mineralogical Association of Canada Short Course series 40.

Hogarth D.D. (1977) Classification and nomenclature of the pyrochlore group minerals. *American Mineralogist*, **62**, 403–410.

Hogarth D.D., Williams C.T. and Jones P. (2000) Primary zoning in pyrochlore group minerals from carbonatites. *Mineralogical Magazine*, **64**, 683–697.

Hornig-Kjarsgaard I. (1998) Rare earth elements in sövitic carbonatites and their mineral phases. *Journal of Petrology*, **39**, 2105–2121.

Jago B.C. and Gittins J. (1993) Pyrochlore crystallization in carbonatites: the role of fluorine. *South African Journal of Geology*, **96**, 149–159.

Kjarsgaard B.A. and Mitchell R.H. (2008) Solubility of Ta in the system $CaCO_3$–$Ca(OH)_2$–$NaTaO_3$–$NaNbO_3$ ± F at 0.1 GPa: Implications for the crystallization of pyrochlore group minerals in carbonatites. *The Canadian Mineralogist*, **46**, 981–990.

Lee M.J., Lee J.L., Garcia D., Moutte J., Williams C.T. Wall F. and Kim Y. (2006) Pyrochlore chemistry from the Sokli phoscorite–carbonatite complex, Finland: implications for the genesis of phoscorite and carbonatite association. *Geochemical Journal*, **40**, 1–13.

Lumpkin G.R. and Ewing R.C. (1995) Geochemical alteration of pyrochlore group minerals: pyrochlore subgroup. *American Mineralogist*, **81**, 1237–1248.

Mitchell R.H. (2004) Mineralogical and experimental constraints on the origins of niobium mineralization in carbonatites. Pp 201–215 in: *Rare Element Geochemistry and Mineral Deposits* (R.L. Linnen and I.M. Samson, editors). Geological Association of Canada, Short Course Notes 17.

Mitchell R.H. (2014) Cathodoluminescence of apatite. Pp.143–167 in: *Cathodoluminescence and its Application to Geoscience* (I.M. Coulson, editor). Mineralogical Association of Canada Short Course 45.

Mitchell R.H. (2015) Primary and secondary niobium mineral deposits associated with carbonatites. *Ore Geology Reviews*, **64**, 626–641.

Mitchell R.H. and Kjarsgaard B.A. (2004) Solubility of niobium in the system $CaCO_3$–$Ca(OH)_2$–$NaNbO_3$ at 0.1 GPa pressure. *Contributions to Mineralogy and Petrology*, **144**, 93–97.

Mitchell R.H. and Platt R.G. (1979) Nepheline-bearing rocks from the Poohbah Lake complex, Ontario: Malignites and malignites. *Contributions to Mineralogy and Petrology*, **69**, 255–264.

Mitchell R.H., Chudy T., McFarlane C.R.M. and Wu F.Y. (2017) Trace element and isotopic composition of apatite in carbonatites from the Blue River area (British Columbia, Canada) and mineralogy of associated silicate rocks. *Lithos*, **286–287**, 75–91.

Nasraoui M. and Bilal E. (2000) Pyrochlores from the Lueshe carbonatite complex (Democratic Republic of Congo): a geochemical record of different alteration stages. *Journal of Asian Earth Sciences*, **18**, 237–251.

Rukhlov A.S. and Bell K. (2010) Geochronology of carbonatites from the Canadian and Baltic Shields, and the Canadian Cordillera: clues to mantle evolution. *Mineralogy and Petrology*, **98**, 11–54.

Sage R.P. (1987) Geology of Carbonatite-Alkalic Rock Complexes in Ontario: Prairie Lake Carbonatite Complex, District of Thunder Bay. *Ministry of Northern Development and Mines, Ontario Geological Survey Study*, **46**, 91 pp.

Walter B.F., Parsapoor A., Braunger S., Marks M.A.W., Wenzel T., Martin M and Markl G. (2018) Pyrochlore as a monitor for magmatic and hydrothermal processes in carbonatites from the Kaiserstuhl volcanic complex (SW Germany). *Chemical Geology*, **498**, 1–16.

Wang L.X., Marks M.A., Wenzel T., Von Der Handt A., Keller J., Teiber H. and Markl G. (2014) Apatites from the Kaiserstuhl Volcanic Complex, Germany: new constraints on the relationship between carbonatite and associated silicate rocks. *European Journal of Mineralogy*, **26**, 397–414.

Witt W.K., Hammond D.P. and Hughes M. (2019) Geology of the Ngualla carbonatite complex, Tanzania, and origin of the Weathered Bastaesite Zone REE ore. *Ore Geology Reviews*, **105**, 28–54.

Wu F.Y., Mitchell R.H., Li Q.L., Zhang C. and Yang, Y.H. (2017) Emplacement age and isotopic composition of the Prairie Lake carbonatite complex, Northwestern Ontario, Canada. *Geological Magazine*, **154**, 217–236.

Wyllie P.J. and Biggar G.M. (1966) Fractional crystallization in the "carbonatite systems" CaO–MgO–CO_2–H_2O and CaO–CaF_2–P_2O_5–CO_2–H_2O. Pp. 92–105 in: *International Mineralogical Association Papers, IMA Volume 1966*, Mineralogical Society of India.

Zurevinski S.E. and Mitchell R.H. (2004) Extreme composition variation in pyrochlore group minerals at the Oka Carbonatite Complex. Québec: evidence of magma mixing? *The Canadian Mineralogist*, **42**, 1159–1168.

Zurevinski S.E. and Mitchell R.H. (2015) Petrogenesis of orbicular ijolites from the Prairie Lake complex, Marathon, Ontario: Textural evidence for rare processes of carbonatitic magmatism. *Lithos*, **239**, 234–244.

https://doi.org/10.1180/mgm.2019.64 Published online by Cambridge University Press